Naval Research Laboratory
Washington, DC 20375-5320

NRL/MR/6722--94-7459

PRS Projections for DECADE

K. G. WHITNEY
J. W. THORNHILL
J. L. GIULIANI, JR.
J. DAVIS

Radiation Hydrodynamics Branch
Plasma Physics Division

April 25, 1994

REPORT DOCUMENTATION PAGE

Form Approved
OMB No. 0704-0188

1. AGENCY USE ONLY (*Leave Blank*)	2. REPORT DATE	3. REPORT TYPE AND DATES COVERED
	April 25, 1994	

4. TITLE AND SUBTITLE

PRS Projections for DECADE

5. FUNDING NUMBERS

6. AUTHOR(S)

K.G. Whitney, J.W. Thornhill, J.L. Giuliani, Jr., and J. Davis

7. PERFORMING ORGANIZATION NAME(S) AND ADDRESS(ES)

Naval Research Laboratory
Washington, DC 20375-5320

8. PERFORMING ORGANIZATION REPORT NUMBER

NRL/MR/6722--94-7459

9. SPONSORING/MONITORING AGENCY NAME(S) AND ADDRESS(ES)

Defense Nuclear Agency
RAEV
Alexandria, VA 22310

10. SPONSORING/MONITORING AGENCY REPORT NUMBER

11. SUPPLEMENTARY NOTES

12a. DISTRIBUTION/AVAILABILITY STATEMENT

Approved for public release; distribution unlimited.

12b. DISTRIBUTION CODE

13. ABSTRACT (*Maximum 200 words*)

Two approaches are described for predicting and evaluating the potential range of PRS performance on DECADE. On the one hand, the DECADE generator is represented as a lumped electrical circuit coupled to an inductive PRS load using slug model dynamics for the load. The nonlinearly coupled circuit equations determine the energy transfer from the Marx bank to the load as a function of the circuit parameters, enabling one to predict the efficiency for converting Marx bank energy into load kinetic energy. Newly experimentally confirmed scaling relations then allow one to predict the conversion fraction of this kinetic energy into K-shell x-rays. Both aluminum an titanium should be able to generate in excess of 100 kJ/cm of K-shell radiation based on the DECADE circuit model used in this report. On the other hand, power flow from the Marx generator to the load is taken as a given, and a number of specific issues related to PRS load dynamics are calculated using detailed (non-slug) models of the load MHD dynamics. A number of such issues are discussed. They need to be addressed because of their potential to either degrade or enhance the load yield performance predicted on the basis of kinetic energy and x-ray scaling laws alone. These issues also deal with matters of x-ray simulation fidelity that will be an important part of DECADE's function. It is argued that the capability to carry out aluminum radiative collapse experiments on DECADE is significantly greater than on existing simulators, and that these experiments may offer a range of opportunity for improving simulation fidelity beyond that offered by kinetic energy scaling alone. This represents a compelling reason for giving DECADE a PRS capability.

14. SUBJECT TERMS

K-shell radiation emission
K-shell yield scaling
PRS load dynamics

15. NUMBER OF PAGES

33

16. PRICE CODE

17. SECURITY CLASSIFICATION OF REPORT	18. SECURITY CLASSIFICATION OF THIS PAGE	19. SECURITY CLASSIFICATION OF ABSTRACT	20. LIMITATION OF ABSTRACT
UNCLASSIFIED	UNCLASSIFIED	UNCLASSIFIED	UL

NSN 7540-01-280-5500

Standard Form 298 (Rev. 2-89)
Prescribed by ANSI Std 239-18
298-102

CONTENTS

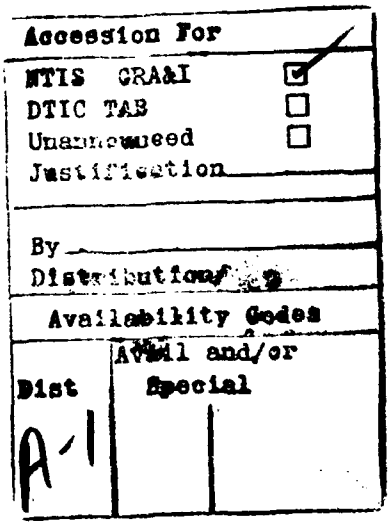

PRS Projections for DECADE

I. DECADE ENERGY CONSIDERATIONS

Designing DECADE for use as a plasma radiation source (PRS) involves two important considerations. One, the efficiency with which the Marx bank couples energy to the PRS load must be realistically evaluated for different DECADE PRS front-end designs. Two, the efficiency of converting coupled electrical energy into K- and L-shell kilovolt radiation must be realistically determined for a variety of load designs and for a selection of low, moderate, and high Z elements. During FY 93, a capability to evaluate the effect of different front-end designs on DECADE Marx bank/PRS coupling efficiency was developed, and a significant advancement was made in our understanding of the scaling of K-shell yields with mass and implosion velocity to DECADE. These developments will be described in this section. The latter advancement was made possible by a (first ever) systematic comparison of theoretically predicted K-shell yields with measured yields on three different pulse-power generators: Double Eagle, Saturn, and Phoenix.

There are two ways to approach the DECADE coupling and scaling problems. They depend on whether emphasis is placed on technical issues associated with the design of multi-megajoule pulse power generators or whether emphasis is placed on issues associated with efficiently converting electrical energy into x rays (especially x rays that are tailored for use in NWET). Historically, *the first approach has dominated DNA thinking, the thought being that if a pulse power machine can be built, then the x rays will come.* For this reason, emphasis has generally been placed on machine problems, and x-ray generation is taken either as a "fait acompli" or as "que sera, sera". A spin-off of this view is that x-ray output is often calculated or estimated on "the back of an envelope". The scaling of non-thermal x rays would appear to reflect this point of view. On the one hand, it is important to propose new experimental schemes, and, thus, it is useful to hunt for non-thermal emission processes in z-pinches. It is equally important to understand how it is these x rays are or need to be generated. On the other hand, one cannot casually predict their scaling. An analogy for understanding the sense of this point of view is to liken the construction of an x-ray simulator to that of a building. The pulse-power generator represents the building's foundation and girding, without them neither the simulator nor the building can exist. The office furniture and equipment corresponds to the simulator user community, both help to define the function and use of the building or simulator. However, the building itself corresponds to the PRS load from which the x rays must come; neither the building layout nor the load physics should be afterthoughts.

The discussion in this report will, at first, put forth a machine approach to DECADE because basic PRS requirements must guide the design of DECADE's PRS front-end just as a building determines the foundation it needs. However, this report will end with a brief discussion of the non-machine, load problems that need to be addressed to maximize DECADE's return on investment as an x-ray NWE simulator. Thus, for example, when x-ray yield scaling is carried out initially over three or more orders of magnitude in order to evaluate the machine requirements for scaling from past and present machines to future machines, a factor of two difference in yields can be ignored. However, when a DECADE- or Jupiter-class PRS machine is built, a factor of two or three difference in performance will be very significant in terms of simulation fidelity and dollars/photon. In both of these simulation fidelity areas, (non-machine) PRS design issues become important.

The machine view of PRS adopted in this report is the following. A PRS load is defined in terms of the amount of mass, m, to be imploded and the initial radius, r_i, from which it is

Manuscript approved February 23, 1994.

imploded. Both of these quantities are assumed to be completely free variables. (There are technological problems associated with this assumption such as how well will gas nozzles work as the load mass and length are increased and how well can wire initial conditions be controlled as the wire mass and length are increased.) A (lumped) circuit model that describes a given DECADE machine is then coupled to the PRS load, and a slug implosion model[1] is used to calculate the kinetic energy imparted to the given load by the given machine. These calculations are stopped at a pre-determined radius (2 mm) and the final implosion velocity, v_{imp}, of the load is determined. The choice of 2 mm is governed by two factors: (1) a larger v_{imp} can be generated the further in the slug implosion proceeds, and (2) less plasma back-pressure is generated to halt the acceleration the further out in the implosion the calculation is stopped. Finally, the results of these calculations are displayed on an m-v_{imp} contour plot.

An example of such a plot is shown in Fig. (1). The darkened crescent region in Fig. (1) represents the span of implosion velocities that were calculated using the circuit model for DECADE that is shown in Fig. (2) for the range of radii and masses shown: 2 cm $\leq r_i \leq$ 3.5 cm and 0.22 mg/cm $\leq m \leq$ 10.6 mg/cm. This darkened region overlaps with three regions that are labeled in Fig. (1) as regions of inefficient, efficient, and inefficient x-ray production respectively. The labeled regions in this figure are for titanium. The figure indicates that titanium loads should be able to efficiently convert implosion kinetic energy to K-shell x rays on DECADE, but only for a certain choice of radii and masses. More will be said to explain the origin of this figure later in this section. The unlabeled K-shell yield contours that are drawn in Fig. (1) are the same as those drawn in Figs. (6)-(8). Thus, Fig. (1) predicts that, at minimum, DECADE should be capable of generating 100 kJ/cm of titanium K-shell radiation or in excess of 300 kJ for a 3 cm length load.

The model in Fig. (2) contains the following basic elements of a DECADE circuit: the Marx generator, C_1, the transfer capacitor, C_2, the transfer switch, R_3, the pulse forming line, L_3, the plasma opening switch (POS), R_{pos}, the magnetically insulated transmission line (MITL) of the PRS diode, L_4, and the PRS load, V_{load}. These elements were given the values shown in the figure. The use of this lumped circuit description of DECADE allows one to compute the efficiency of converting the initially stored energy of the Marx bank, E_{Marx}, into PRS kinetic energy. For example, for the same range of masses and load radii that were used to obtain the span of implosion velocities shown in Fig. (1), one obtains the corresponding span of Marx-bank-to-load-kinetic-energy conversion efficiencies shown in Fig. (3) (for a 3 cm long array). The boundaries in Fig. (3) are labeled and are in one-to-one correspondence with the boundary labeling of Fig. (1). Also, the line drawn through the shaded portion of the efficient region in Fig. (1) corresponds to the line through the shaded region in Fig. (3). The latter line demonstrates that the efficiency for converting Marx bank energy into kinetic energy increases from 8% to 14% when the load mass is increased from 0.7 mg/cm to 1.3 mg/cm for a fixed implosion velocity of $\sim$80 cm/μsec. For the Fig. (2) circuit, the largest mass loads, $m \sim$ 10 mg/cm, are also the most efficient converters of Marx energy into kinetic energy ($\sim$ 15% $-$ 17%). In electrical engineering terms, these loads are optimally matched (or coupled) to the DECADE circuit. Several years ago, experimenters used this criterion to design their PRS experiments, but, as Fig. (1) shows, this mass of titanium on DECADE is an inefficient K-shell radiator. Efficient emission occurs for 0.6 mg/cm $\leq m \leq$ 1.8 mg/cm. For these masses, the conversion efficiency of Marx bank energy to kinetic energy is between 8 and 15%.

One can anticipate that, at the present moment under optimum conditions, 30 to 50% of

the kinetic energy generated during a PRS implosion can be converted into K-shell x rays in the efficient x-ray production region of $m - v_{imp}$ space. This point is discussed more fully later in this section. By multiplying together the above two conversion efficiencies, one concludes that 2.4% to 7.5% of the Marx bank energy can be converted to K-shell x rays by the Fig. (2) circuit model (8% to 15% $\times$ 30% to 50%). Since $E_{Marx} = 8.5$ MJ, these basic considerations alone predict that the DECADE machine of Fig. (2) should be able to produce between 200 to 640 kJ of titanium K-shell radiation. Here we have an example of a factor of three in x-ray output that could be extremely important to the simulator users community.

II. K-SHELL SCALING

The basic idea of K-shell scaling is that two implosion kinetic energies determine the radiation characteristics of PRS loads: (1) the kinetic energy per ion, $K_i \equiv (1/2)m_i v_{imp}^2$, and the kinetic energy per centimeter, $K_c \equiv (1/2)m v_{imp}^2$, where m_i is the mass of an ion. In order to efficiently convert z-pinch kinetic energy into x rays, K_i must be larger than a predetermined minimum energy, E_{min}, which one can estimate by the formula, $E_{min} \cong 1.012 Z^{3.662}$, if one ignores kilovolt radiation L-shell losses. Z is the atomic number of the PRS load. Since efficient K-shell radiation is emitted per ion in units of E_{min}, it is convenient to define a dimensionless kinetic energy per ion, η, defined by $\eta \equiv K_i / E_{min}$.

Our present understanding of K-shell yield scaling evolved over a period of the last five years from a concerted theoretical and experimental effort between NRL and Physics International, Co.. Roughly speaking, it involved the following five separate steps:

1. A simple slug model theory of K-shell yield scaling was developed. It was then used to plan a set of 1-D radiative hydrodynamics implosion calculations that would systematically quantify the radiative capabilities of a z-pinch. Current flow in these calculations was turned off just before the load assembled on axis in order to determine the efficiency of thermalizing the kinetic energy and of converting this energy into K-shell x rays. These calculations utilized the full capability, which had been developed over the preceding ten years, of Code 6720 to model the radiative behavior of imploding z-pinches realistically. Consequently, The reliability of the calculations was high. Two kinds of calculations were carried out:
   a) m was held constant and η was varied
   b) η was held constant and m was varied.
2. Aluminum (and later argon) was chosen for a detailed theoretical PRS load analysis. It was expected that existing simulators could then be used to test the theoretical predictions of these calculations, i.e., it was apparent that existing simulators had enough current to efficiently ignite the K-shell of aluminum, but not enough to efficiently ignite higher Z elements.
3. The results from these calculations, when plotted on a log-log graph, showed there were roughly two scaling regimes of K-shell yield with mass (ignoring factors of two or more). Moreover, these regimes made sharp transitions into one another. Because of the qualitative nature of these results, they could be scaled with Z and used to predict the machine requirements for producing K-shell radiation from elements having atomic numbers higher than aluminum.
4. Detailed comparisons were next made of the calculated z-pinch results with carefully analyzed experimental spectral data.[2] Consequently, it was found that the calculations predicted much

harder implosions than were seen experimentally, i.e., the calculated ion densities on axis were two or more orders of magnitude larger than the inferred experimental densities.

5. The calculations were then modified by enhancing the plasma viscosity, the heat conductivity, and the electrical resistivity through the use of multiplicative factors. These enhancements mimicked the effects of plasma turbulence, assuming its presence due to, for example, the finite number of return current posts. They were found to soften the implosions and to produce much better agreement between theory and experiment for both argon[3] and aluminum[2] than had been obtained without their use. They also had the important effect of significantly modifying the scaling predictions.[4]

This newly modified scaling relation is used later in this section to analyze two sets of recently completed Saturn and Phoenix aluminum experiments. They were designed specifically for these machines. The analysis of these experiments has led to the development of a new, and more simplified, scaling relation with which to predict DECADE performance from kinetic energy scaling considerations alone.

The basic mathematical results of the scaling work can be found in Ref. (5). We summarize them briefly here:

(1) For small masses, K-shell x-ray yield, y_K, scales quadratically with mass:

$$y_K = am^2. \tag{1}$$

(2) For large masses, it scales as

$$y_K = bm. \tag{2}$$

(3) The coefficients, a and b, are functions of Z and η.

(4) The intersection of the two yield curves defines the breakpoint mass, m_{BP}, and the breakpoint yield, y_{BP}:

$$m_{BP} = \frac{b}{a} \qquad y_{BP} = \frac{b^2}{a}. \tag{3}$$

A dependence of the coefficients, a and b, on Z and η was worked out in Ref. (5). In detail, the scaling relations are:

$$m_{BP}(\mu g/cm) = \frac{f_K b_0 Z^{5.96}}{a_0 E(Z)}, \tag{4}$$

$$y_{BP}(kJ/cm) = \frac{f_K^2 b_0^2 Z^{8.37}}{a_0 E(Z)}, \tag{5}$$

where f_K is the fractional conversion efficiency of kinetic energy to K-shell radiation in the efficient region. We conservatively take it to be 0.3 when we use Eqs. (1) and (2) to plot yields on figures such as Fig. (1). The exponential factor, E, is given by

$$E(Z) \equiv \exp\left(-20.6/Z^{0.9}\right), \tag{6}$$

and the coefficients, a, b, a_0, and b_0, by

$$a = a_0 E(Z) Z^{-3.55} \qquad b = f_K b_0 Z^{2.41}, \tag{7}$$

where

$$a_0(kJcm/\mu g^2) = \frac{1}{6}\left(33.7 + \frac{595}{\eta} - \frac{70.7}{\eta^2}\right) \tag{8}$$

and

$$b_0(kJ/\mu g) = 9.1 \times 10^{-5}\eta. \tag{9}$$

Following their derivation, the scaling predictions were checked against a series of nickel hard implosion calculations carried out for $\eta \cong 4$. These results were documented in Ref. (6). Eq. (4) predicts that $m_{BP} \cong 800$ μg/cm. This value is much higher than the value of 100 μg/cm that was calculated because of nickel L-shell emissions. However, at 800 μg/cm in these calculations, nickel K-shell emissions began to dominate over the L-shell emissions. These were hard implosion calculations; consequently, they are probably less realistic for nickel loads than they were for aluminum. Soft implosion modeling needs to be done to better understand the Z dependence of K-shell yield scaling. This work will be carried out in the near future.

The analysis in Ref. (4) showed that soft implosions shift the mass breakpoint and soften the transition between m^2 and m scaling. The correction factor of $\sim$1/6, which is included in the equation for a_0, comes from this analysis. It increases m_{BP} by a factor of 6. Fig. (4) illustrates this effect for argon. The soft implosions that were calculated with this particular turbulence model require $\sim$6 times the argon mass as the hard implosions before they reached the same, linear in m, scaling regime as the hard implosions had.

The above discussion laid out two requirements to be satisfied to achieve efficient emission of K-shell x rays from different elements. On the one hand, one must have $\eta > 1$ (preferably $\eta > 2$). On the other hand, one must have $m \geq m_{BP}$. The curves, η =constant and $m = m_{BP}$, define the boundaries of an efficient K-shell emission region in $m - v_{imp}$ space. The consequence of these two requirements is shown in Fig. (5) (also in Ref. (7)). Two shaded regions are shown. They represent the portions of $m - v_{imp}$ space from which efficient emission is expected from the K-shells of aluminum and krypton. Note that the lower boundary curves are defined by $\eta = 1.5$. Fig. (5) quantifies the significantly increased mass and implosion velocity requirements for krypton to radiate efficiently in the K-shell than those of aluminum.

While the shaded regions in Fig. (5) indicate where efficient x-ray production is expected, they do not show how the yield increases as K_c (i.e., m or v_{imp}) increases. This information can be obtained from Eqs. (1),(2), and (6)-(9), and it can be displayed as contours on an $m - v_{imp}$ plot. Contours for 10, 30, 100, 300, 1000, and 3000 kJ/cm yields are shown in Figs. (6) and (7) for aluminum and copper respectively. Fig. (6) also contains two data points, one from Double Eagle and one from Saturn. These data indicate that experiments on present-day machines have already exceeded the yields that are predicted by Eqs. (1) and (2) when $f_K = 0.3$. Part of the reason for the conservative yields predicted by our model is related to the fact that no post-stagnation energy coupling is included in the model as yet.

III. THEORY VERSUS EXPERIMENT

Because of two series of aluminum experiments that were recently completed at Sandia National Laboratories and at NSWC on the Saturn and Phoenix machines respectively, it is now possible to test the yield predictions of Fig. (6) over two different spans of m and v_{imp} in $m - v_{imp}$

SATURN PRS Experiments

Wire Diam (mil)	Wire Mass (μg/cm)	Array Diam (cm)	η	Wires #	K.E. kJ	Yield kJ	C.E. %
0.6	120	3.04	22	24	230	8.0	3.5
0.7	160	2.81	17	24	230	12.2	5.3
0.75	185	2.73	15	24	230	22.4	9.7
1.0	330	1.72	6.0	24	170	76.0	44.7
1.2	470	2.29	5.6	24	230	61.2	26.6
1.5	740	1.46	2.7	24	170	30.0	17.6
1.7	950	1.4	2.2	24	170	20.0	11.8
2.0	1310	1.34	1.6	24	170	14.2	8.4
2.5	2050	1.25	0.95	24	170	4.9	2.9

space. The Saturn experiments were performed at the end of FY92. The highest yielding of the different mass Saturn experiments are listed below. Each aluminum array had a length of 2 cm.

In each of these experiments, 24 wires of different, but standard, wire diameters were mounted at the various array diameters listed in the table. The total kinetic energies and the η values that are listed were computed from a slug model using the Saturn lumped circuit as its driver. Each kinetic energy calculation was terminated at a radius of 1.5 mm. The (K-shell) total yields listed in the table were measured, and each percent conversion efficiency (C.E.) is the ratio of measured yield to computed kinetic energy in each experiment. Two similar sets of experiments were designed and carried out at Phoenix in FY93, a set of 3 cm long array experiments and a set of 2 cm long array experiments (for which, again, only the highest yielding shots are listed):

Phoenix Aluminum Experiments

array length = 3 cm

Wire Diam (mil)	Wire Mass (μg/cm)	Array Diam (cm)	η	Wires #	K.E. kJ	Yield kJ	C.E. %
0.8	140	2.9	5.1	16	92	21.8	24
1.2	158	2.4	3.9	8	79	26	33
1.0	219	2.6	3.5	16	99	23	23
1.0	219	2.2	3.0	16	84	13	15
1.5	246	2.3	2.9	8	94	26	28
1.5	246	1.85	2.2	8	70	17	24
1.2	315	1.95	2.0	16	82	13.0	16

Phoenix Aluminum Experiments

array length = 2 cm

Wire Diam (mil)	Wire Mass (μg/cm)	Array Diam (cm)	η	Wires #	K.E. kJ	Yield kJ	C.E. %
0.6	79	2.62	7.0	16	46	8.6	18.7
0.7	107	2.58	5.7	16	52	19.5	37.5
0.8	140	2.25	4.05	16	48.5	26	54
1.2	158	2.35	3.8	8	52	21.7	41.7
1.0	219	2.1	2.6	16	55	18	33
1.5	246	1.9	2.2	8	46	22.9	49.8
1.6	280	2.0	2.0	8	49	21	43
1.2	315	2.26	2.2	16	60	14.7	24.5
1.6	560	1.15	0.6	16	31	6.5	21

The last columns in these tables show that the experiments were completed with mixed success. The 2 cm experiments had large conversion efficiencies (many larger than 0.3), and the 3 cm experiments did not (all but one smaller than 0.3). Some unknown machine problems may have been experienced with the 3 cm long loads, but they were never confirmed. They were suspected since the 3 cm loads had conversion efficiencies below those achieved in the past with 4, 5, and 6 cm long loads. By contrast, in the 2 cm load experiments, the earlier 4, 5, and 6 cm conversion efficiencies were exceeded. These experiments also indicated that the circuit model that was used in their design needed recalibration. The voltage driver had to be reduced by 10% to compute the kinetic energy values listed in the table.

Both the Saturn and Phoenix experiments were designed to probe through the efficient K-shell emission region in Fig. (6). Their specific location is shown in Fig. (8) along with contours for predicted K-shell yields. The nine dots represent the nine 2 cm load Saturn experiments and the nine triangles, the nine 2 cm load Phoenix experiments. The K-shell yields that were measured in each of these experiments are plotted in Figs. (9) and (10) respectively. Interestingly, the maximum yield was recorded in the experiment that lay within the efficient region but closest to the $m = m_{BP}$ boundary curve in both Saturn and Phoenix experiments. Moreover, as predicted, the yields fell as the experiments generated more implosion velocity, but moved further from the efficient region. Similarly, as the implosion velocity was decreased and the experiments moved in the direction of and ultimately below the $\eta = 1$ lower boundary line, the yields fell. The yield contours that are drawn in Fig. (8) were derived from hard implosion calculations (corrected only for the mass breakpoint shift) and do not show the drop in yield with η that is seen in the data. However, soft implosion calculations do show this trend.

An important difference showed up between the Phoenix and the Saturn data. In all of the six Phoenix shots that lay within the efficient region, the percent conversion of kinetic energy into K-shell x rays was greater than the theoretically conservative value of 30%. For Saturn, however, only the maximum yielding of the five experiments within the efficient region exceeded 30%.

Nevertheless, in this one case, the Saturn conversion efficiency of 45% was close enough to the Phoenix maximum conversion efficiency of 54% to lie within the experimental variation of the two machines.

A tentative, but useful, conclusion can be drawn from the location of the maximum yielding of the Saturn and Phoenix experiments. Since they both lie close to the curve, $y_K = y_{BP} \equiv y_K(m)|_{m=m_{BP}} \equiv y_{BP}(m_{BP})$, one can use this curve to predict an optimal aluminum performance for DECADE. Fig. (5) shows the $y = y(m_{BP})$ curves do not depend strongly on Z. A least squares fit produces the formula,

$$y_K = 0.0056 m^{1.514}, \tag{10}$$

when $f_K = 0.5$. This curve is drawn in Fig. (11), and the Phoenix and Saturn data points that represent the maximum yielding experiments are included on the figure. The DECADE and Jupiter points were placed on the curve by choosing the largest mass that can be accelerated to the breakpoint velocity by these machines. For DECADE, this mass was taken from Fig. (1).

IV. PRS ISSUES

When a simple notion, like the slug model, of PRS load dynamics is adopted, one can draw useful, basic conclusions about the way pulse-power generators should be built to power PRS x-ray simulators. However, these are idealized dynamics that serve only to determine the minimum energy requirements of these machines. For example, for a Jupiter-class generator, initial analysis shows that roughly 10% of the total radiation is emitted during run-in. This radiation affects inductances (load radii) and power flow. Slug model calculations miss these features of the implosion dynamics. Other non-machine, load oriented issues must also be addressed in order to realize a given machine's inherent capabilities and to optimize its performance as an NWE simulator. We will briefly discuss some of these issues, and mention some of the work that was done this year in addressing them. They are subsumed under the following four topics:

- PRS Initial Conditions
- PRS On-axis Symmetry and Implosion Stability
- 20 to 30 KeV Photons
- Radiative Collapse

Each of these topics will be discussed briefly in turn.

A. PRS Initial Conditions

Two basic assumptions underlie the scaling calculations described above. All of the hydrodynamics calculations begin with a given mass of pre-ionized cylindrically symmetric plasma located, on average, at the initial position of a wire array. They assume, therefore, (1) that the power flow from the pulsed-power machine can be coupled to the wire load uniformly to ionize it quickly and (2) that the implosion then takes place with all of the wire mass imploding inwards as described by a slug model driven by the $\mathbf{j} \times \mathbf{B}$ forces of the current discharge. These assumptions are not always justified. There are strong indications that large diameter wires do not ionize uniformly, that some of the wire mass is left behind in the implosion, and that the mass is driven in under a combination of slug and snowplow dynamics. Fig. (12), for example, is a collection of aluminum yield data from three machines shown as a function of the array initial

wire diameter. The clustering of the maximum yield data around 1 mil wires strongly suggests an influence of the wire initial conditions on the wire implosion dynamics. The snowplow influence on aluminum wire array yield data was shown in an analysis of Double Eagle data that was carried out this year.[4] Thus, as machine power is increased, the problem of evaluating the initial response of a wire load to the current pulse could be the most significant part of the power flow problem.

Other evidence was found this year to suggest the importance of the initial breakdown response of a PRS load to the overall performance of the x-ray simulator. It is presented in Figs. (13) and (14). In Fig. (13), the Saturn yield data, discussed above, is plotted as a function of array diameter. This figure also includes Double Eagle data. The dip in the Saturn yield at an array diameter of 2.2 cm is correlated to the rise in the wire ion density generated halfway into the current rise by the wire explosion. A self-similar hydrodynamics model was used to calculate the explosion dynamics. It assumed that the wire expansion was uniform and that this expansion was driven by a time evolving isothermal plasma. This work is described in greater detail in Ref. (8).

B. PRS On-axis Symmetry and Implosion Stability

As machine power is increased, the initial diameter of a PRS array will also need to be increased for several reasons. Large radii implosions reduce some of the difficulties in getting power to flow initially into the diode and couple effectively to the PRS. They also reduce the difficult requirement for a fast rising current pulse. Finally, they should also allow higher aspect ratio (i.e. larger ratios of initial to final array diameter) implosions to be achieved. Increases in this ratio will translate into increases in v_{imp} and to a greater likelihood that the K-shell of high Z elements can be ignited by these implosions.

As array diameters are increased, however, it could become increasingly more difficult to maintain the symmetry of the implosion, which is critical for achieving tight, high density implosions on axis. High density is important for efficient x-ray production. One of the impediments to driving symmetrical implosions is the finite number of return current posts that have been used to date.[9] They automatically destroy cylindrical symmetry, and they may support the generation of plasma turbulence, which, in turn, softens the pinch and makes x-ray production more difficult. Current and load asymmetries will also lead to 2-D plasma flow effects and to Rayleigh-Taylor instabilities.

Whether or not, and by how much, load instabilities and asymmetries degrade radiation yield is an open question. The present situation can be summarized as follows. 2-D fluid calculations will be useful for studying 2-D flow effects in large aspect ratio implosions and for determining conditions for increasing implosion stability and on-axis symmetry with structured large diameter loads. 2-D fluid calculations could also be of use in initiating investigations of plasma turbulence, a process not present in 1-D fluid calculations. However, 3-D calculations are needed if one is to accurately track the late time evolution of turbulence. They are also needed to accurately investigate the nonlinear evolution of Rayleigh-Taylor instabilities and their transition to turbulent flow. If large radius implosions are turbulent (from finite numbers of return current paths, current driven vorticity generation, or Rayleigh-Taylor instabilities), then one might suppose that turbulence's main effects are already being modeled in our 1-D calculations through the use of multipliers for viscosity, heat conductivity, and electrical resistivity. If this is the case, then one might presume that some of the effects of Rayleigh-Taylor instabilities on x-ray yield are already being accounted for in the revised scaling laws. An important question for large radius implosions, therefore, is: will Rayleigh-Taylor cause 2-D average flow defects to form and how deleterious

will they be to x-ray production? If these effects can be studied and understood, then it should be possible, in principle, to mitigate them.

C. 20 to 30 KeV Photons

There are three basic processes by which plasmas radiate; namely, bound-bound, free-bound, and free-free. The latter process is also known as bremsstrahlung emission. Bound-bound emission comes in two forms: line emission from valence electrons or line emission from inner-shell transitions. The relative strength of these processes in a PRS plasma is valence bound-bound >> free-bound >> free-free $\sim$ inner-shell line. Two examples of free-bound emission are shown in Figs. (15) and (16), which contain power spectra for selenium and argon, respectively, that were obtained during the course of 1-D MHD implosion calculations. Notice that the K-shell lines, located at 10 to 15 keV for selenium and at 3 to 4.5 keV for argon, sit on top of two free-bound continua. Also notice that the continuum formed by the recombination of a totally ionized selenium or argon ion to the hydrogen-like ground state extends to 100 keV in Fig. (15) and to 10 keV in Fig. (16). A dashed line is drawn in Fig. (16) to indicate that if the argon plasma had been hotter (and confined), this free-bound continuum would extend to 20 and 30 keV and beyond in a thermal plasma. Thus, a hot, dense, confined argon plasma would be an ideal source for 20 to 30 keV photons for NWET (on DECADE?).

D. Radiative Collapse

The K-shell scaling ideas, developed to date, are based on 1-D hydrodynamics calculations in which the current is terminated when the load assembles on axis to radii where early slug model calculations were terminated. These current-off calculations have the utility of making kinetic energy the principle energy input to the plasma so that the calculated x-ray conversion efficiencies pertain only to kinetic energy conversion. In experiments, however, the current does not turn off, and it will be necessary to extend the scaling laws utilizing current-on calculations. Maintaining the current not only increases the confinement of the pinch, but it can also lead to its radiative collapse. Both of these phenomena can lead to enhanced radiative output. They may also be essential to the effective production of x rays in the 20 to 30 keV energy range.

During FY93, preliminary work was done laying a foundation for current-on PRS investigations. Figs. (17) and (18) show the relevance of current-on calculations to DECADE. Because of its large current, DECADE will have the capability of accelerating a much wider range of aluminum masses into the efficient scaling regime, depending on the initial radius, r_i, of the aluminum array, than existing simulators have. This point is illustrated by the shaded region drawn in Fig. (17). The vertical line, drawn at 0.8 mg/cm as an example, shows how DECADE will provide a capability to map out the dependence of K-shell yield scaling on η for fixed m. This broad capability is not available on currently operational PRS simulators. Fig. (17) also shows that DECADE should provide a capability of exploring radiative collapse behavior over a range of masses from 0.3 to 1 mg/cm.

V. SUMMARY

The role of kinetic energy in the implosion dynamics will be much more varied in DECADE than for existing PRS simulators. Fig. (18) illustrates this point. This figure is to Fig. (17) as Fig. (3) is to Fig. (1). The numbers that label the boundaries in Figs. (17) and (18) are in one-to-one

correspondence. For example, the implosions between 0.1 and 1.0 mg/cm that lie along boundary 4 in Fig. (17) convert only a small fraction (~3 to 4%) of the Marx bank energy into kinetic energy. A substantial portion of the Marx energy may be available, therefore, to drive implosions that are Ohmically heated or that radiatively collapse on axis. *One cannot overemphasize the importance of giving DECADE a PRS capability in order to carry out experiments of this type. They could be critical to achieving enhanced simulation fidelity capability. These experiments would then represent an important first step away from a focus on yield to wider concerns about x-ray simulator performance. DECADE might then become the world's highest fidelity simulator as well as the world's largest pulse power machine.*

Acknowledgement

The Phoenix data, especially for the 3 cm length loads, is presented in this report for documentation purposes. It was obtained at the Naval Surface Warfare Center through the efforts of L. A. Miles, E. E. Nolting, V. L. Kenyon, W. A. Speicer, J. A. Draper, C. R. Parsons, and P. Dang, whose collaboration we benefited from and greatly appreciate.

References

1. J. Katzenstein, J. Appl. Phys. **52**, 676 (1981).
2. C. Deeney, T. Nash, R. R. Prasad, L. Warren, K. G. Whitney, J. W. Thornhill, and M. C. Coulter, Phys. Rev. A **44**, 6762 (1991).
3. C. Deeney, P. D. LePell, B. H. Failor, J. S. Meachum, S. Wong, J. W. Thornhill, K. G. Whitney, and M. C. Coulter, J. Appl. Phys. , to be published.
4. J. W. Thornhill, K. G. Whitney, C. Deeney, and P. D. LePell, Phys. Plasmas **1**, February, (1994), to be published.
5. K. G. Whitney, J. W. Thornhill, J. P. Apruzese, and J. Davis, J. Appl. Phys. **67**, 1725 (1990); J. W. Thornhill, K. G. Whitney, and J. Davis, J. Quant. Spectrosc. Radiat. Transfer **44**, 251 (1990).
6. "Advanced Concepts Theory Annual Report 1990, Final Report", NRL Memorandum Report 6870 (1991).
7. K. G. Whitney, J. W. Thornhill, and J. Davis, "Basic Recommendations for PRS Simulator Design", NRL Memorandum Report 6873 (1991).
8. K. G. Whitney, J. W. Thornhill, R. B. Spielman, T. J. Nash, J. S. McGurn, and L. E. Ruggles, "Analysis of Recent Saturn Aluminum PRS Experiments", Proceedings of the 3-rd International Conference on Dense Z-pinches, London, England (1993), to be published.
9. "Advanced Concepts Theory Annual Report 1992, Final Report", NRL Memorandum Report 6722-93-7301 (1993).

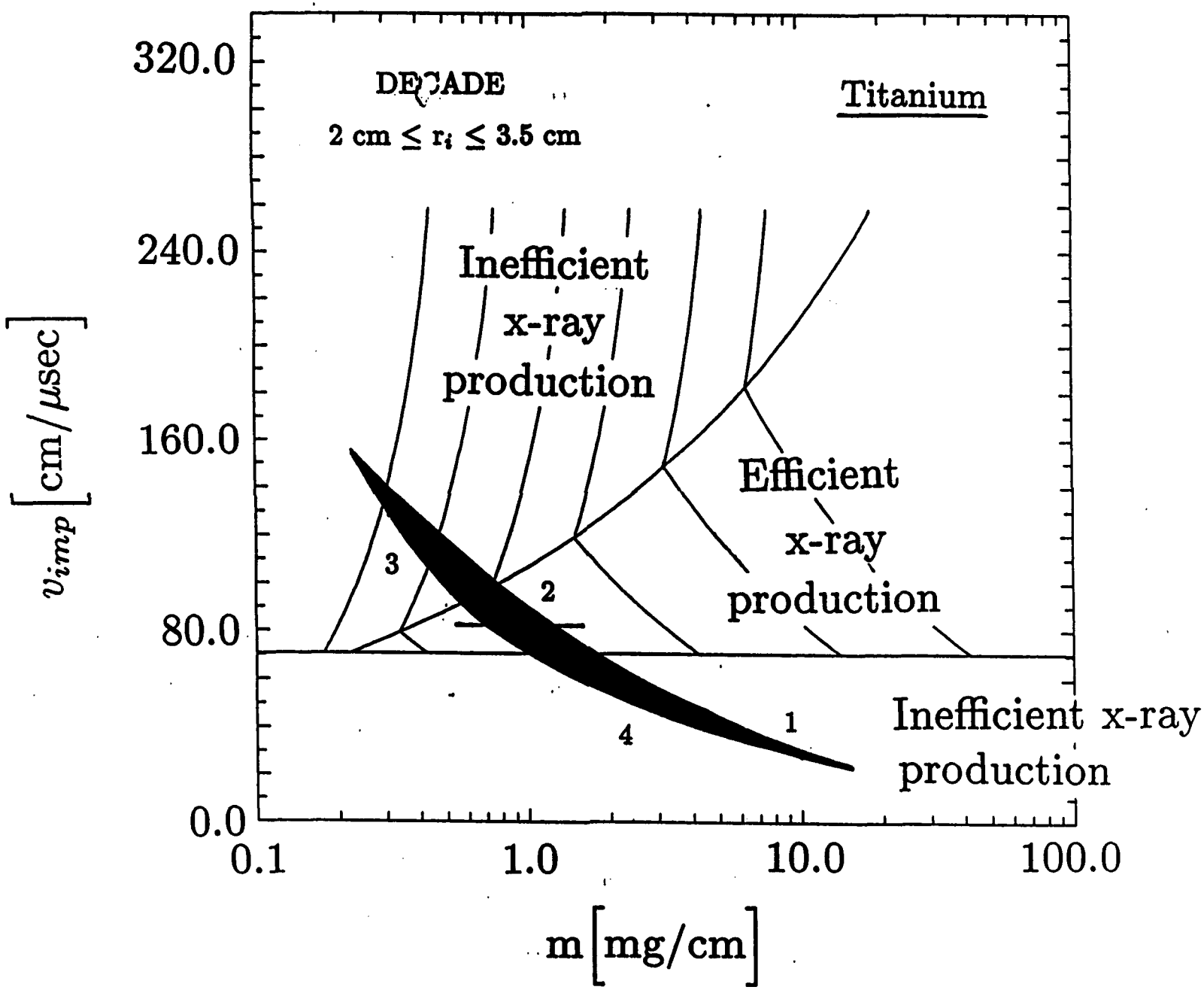
DECADE
2 cm ≤ r_i ≤ 3.5 cm
Titanium
Inefficient x-ray production
Efficient x-ray production
Inefficient x-ray production
1
2
3
4
320.0
240.0
160.0
80.0
0.0
0.1
1.0
10.0
100.0
v_imp [cm/μsec]
m [mg/cm]

Fig. 1

DECADE CIRCUIT MODEL

Transfer Capacitor

Marx Generator Transfer Switch

Pulse Forming Line

Diode MITL

POS PRS Load

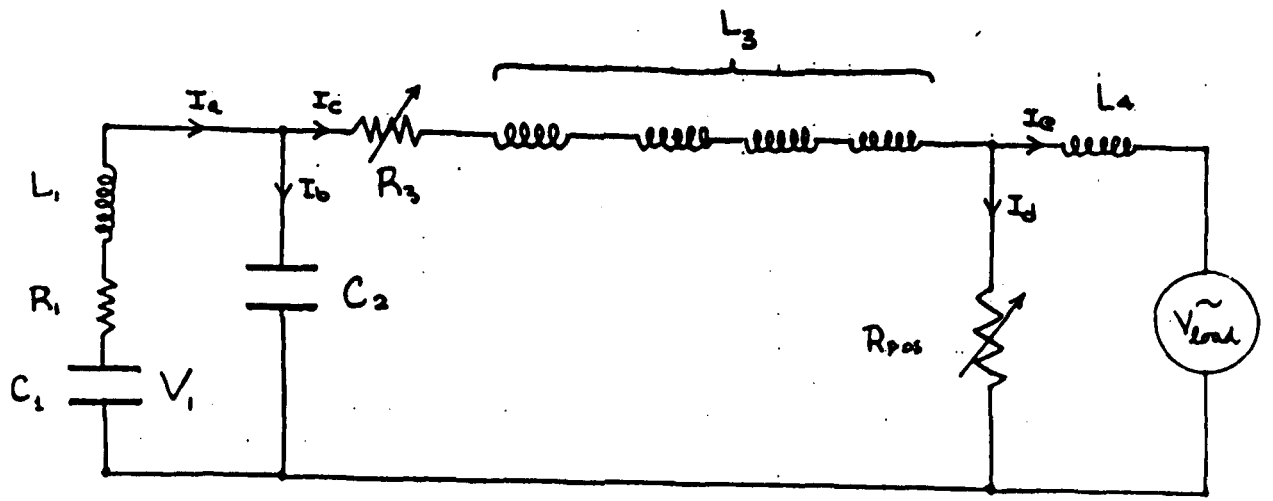

Equivalent Lumped Circuit

$C_1 = 21.12\mu F$ $L_1 = 17.7nH$ $L_3 = 9.92nH$

$V_1 = 0.87MV$ $C_2 = 23.6\mu F$ $L_4 = 4.0nH$

$R_1 = 2.56m\Omega$ $R_3 = 100\Omega \rightarrow 0.125m\Omega$ $R_{POS} = 0.1m\Omega \rightarrow 0.17\Omega$

Fig. 2

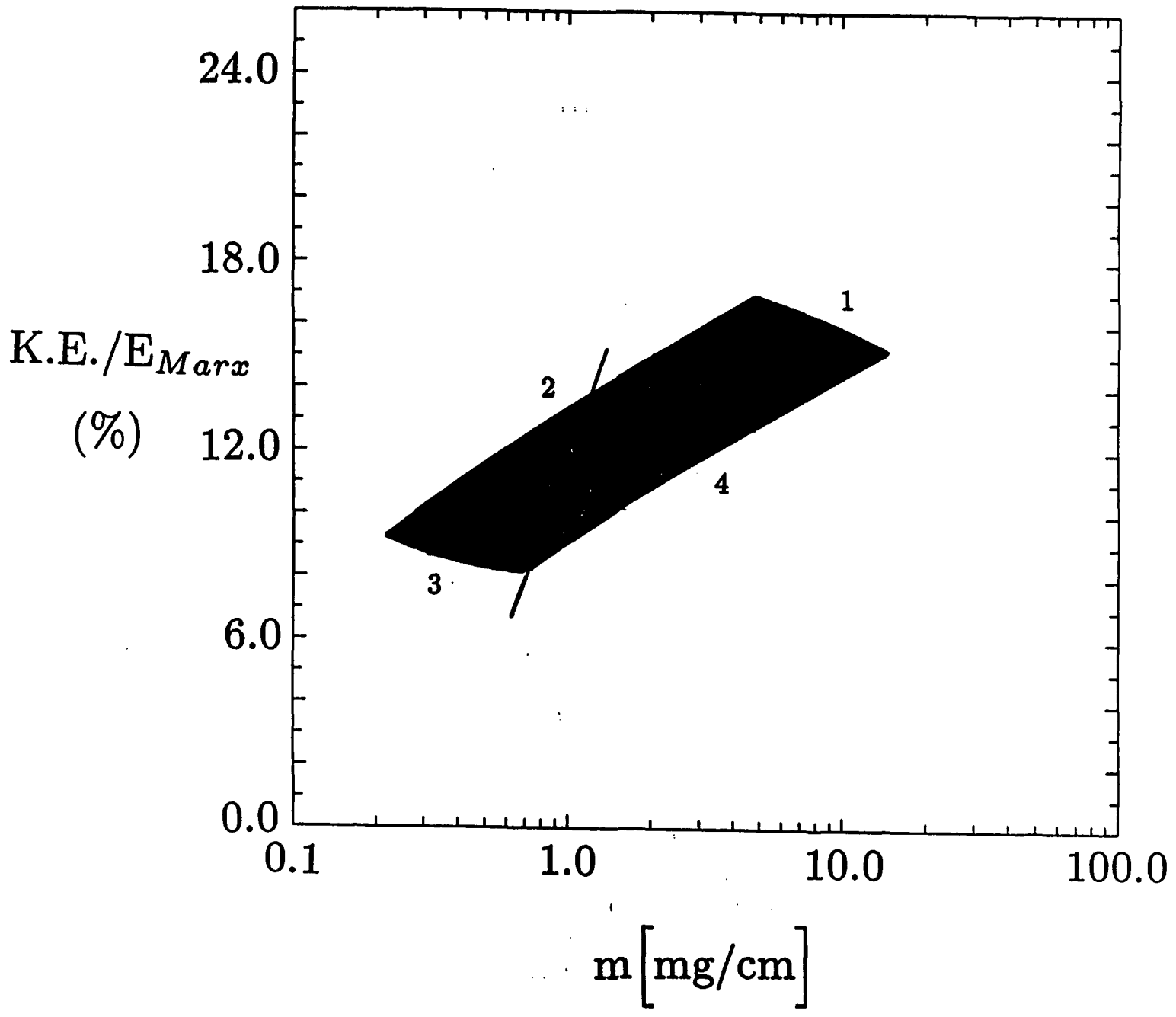

Fig. 3

THE MASS BREAKPOINT SHIFTS AS THE IMPLOSION SOFTENS

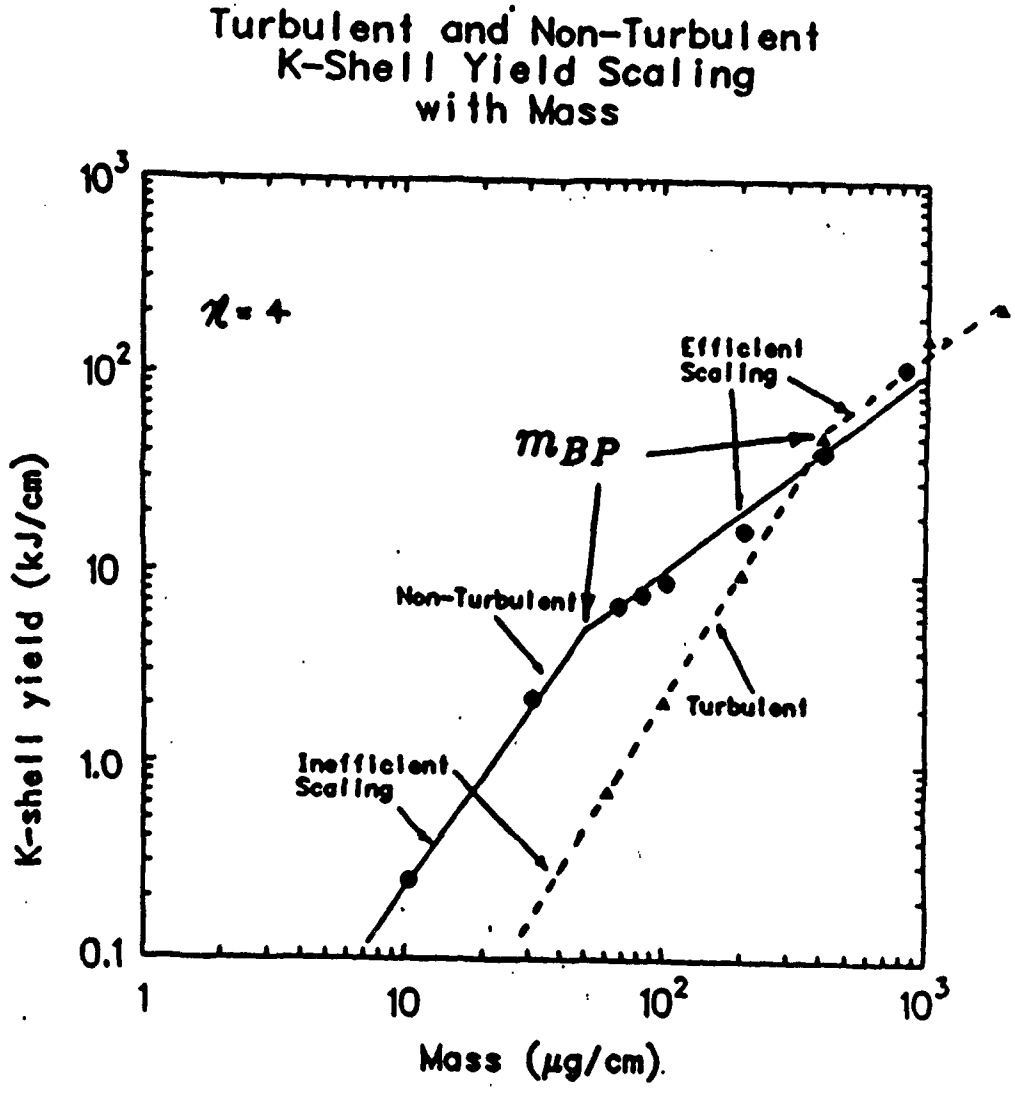

NRL
Code 6720

Fig. 4

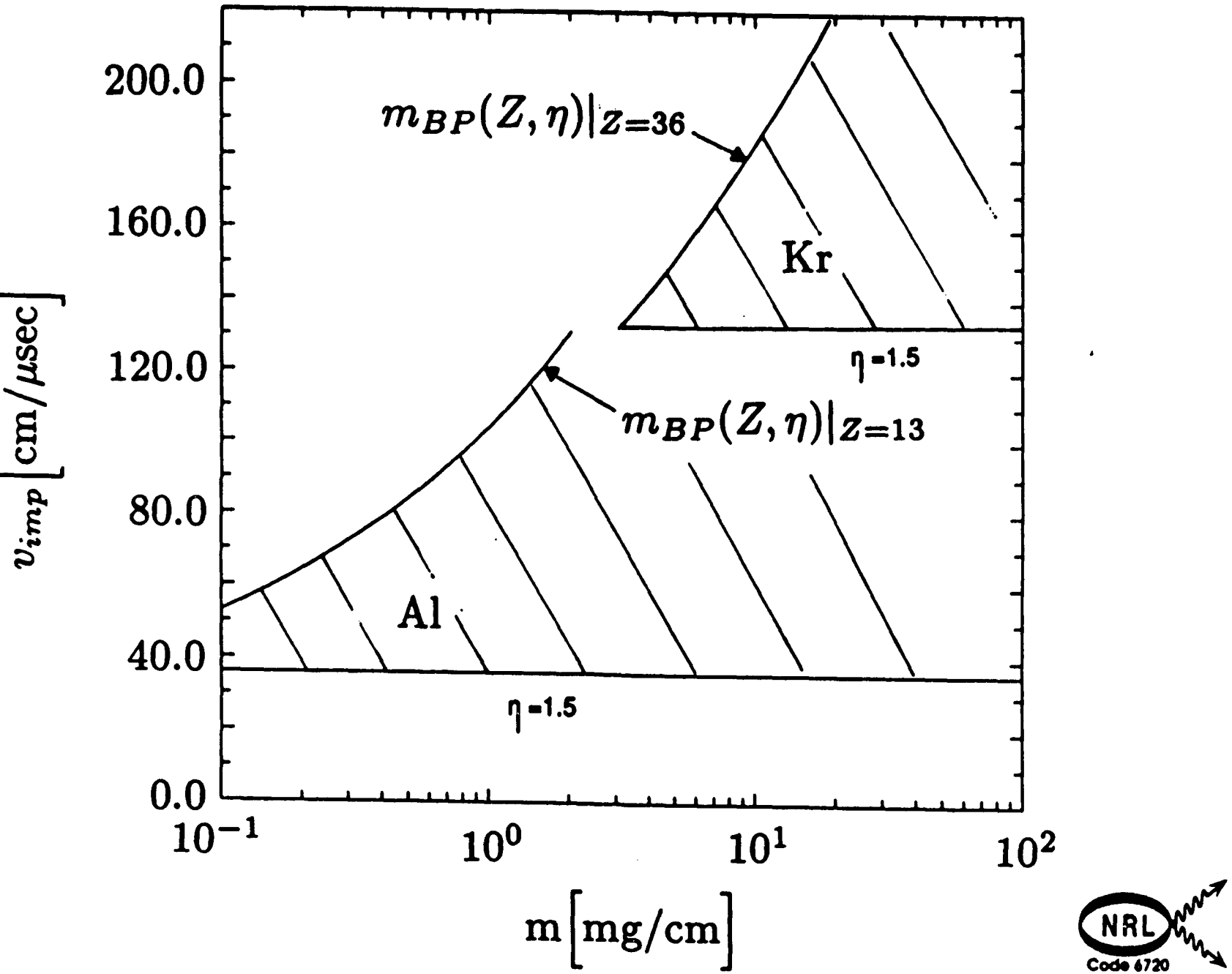
200.0
160.0
120.0
80.0
40.0
0.0
$v_{imp}\left[\mathrm{cm}/\mu\mathrm{sec}\right]$
$m_{BP}(Z,\eta)|_{Z=36}$
Kr
η=1.5
$m_{BP}(Z,\eta)|_{Z=13}$
Al
η=1.5
10^{-1}
10^{0}
10^{1}
10^{2}
m[mg/cm]
NRL
Code 6720

Fig. 5

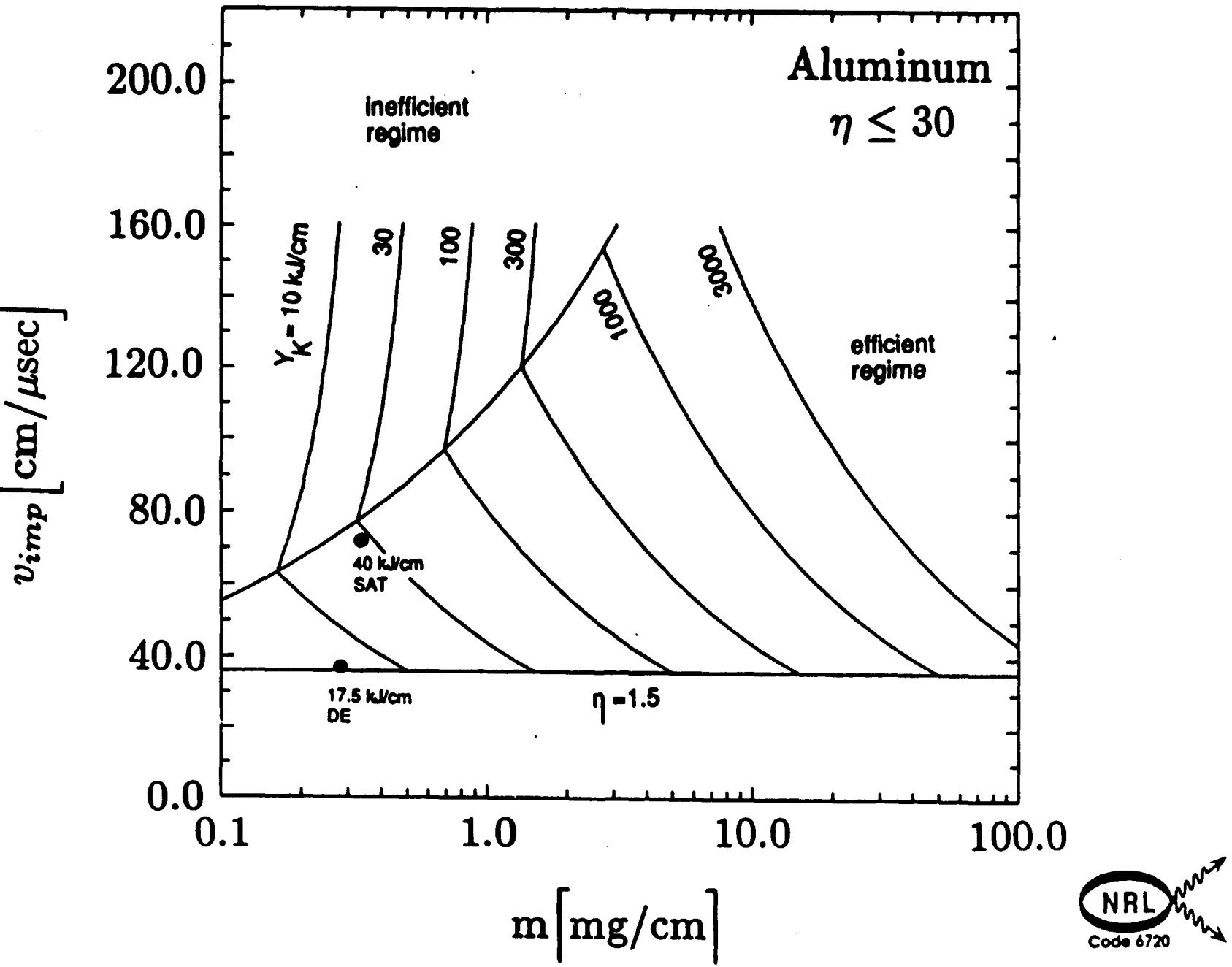
Aluminum
$\eta \leq 30$
inefficient regime
efficient regime
Y_K = 10 kJ/cm
30
100
300
1000
3000
40 kJ/cm SAT
17.5 kJ/cm DE
η =1.5
200.0
160.0
120.0
80.0
40.0
0.0
0.1
1.0
10.0
100.0
v_{imp} [cm/μsec]
m [mg/cm]
NRL
Code 6720

Fig. 6

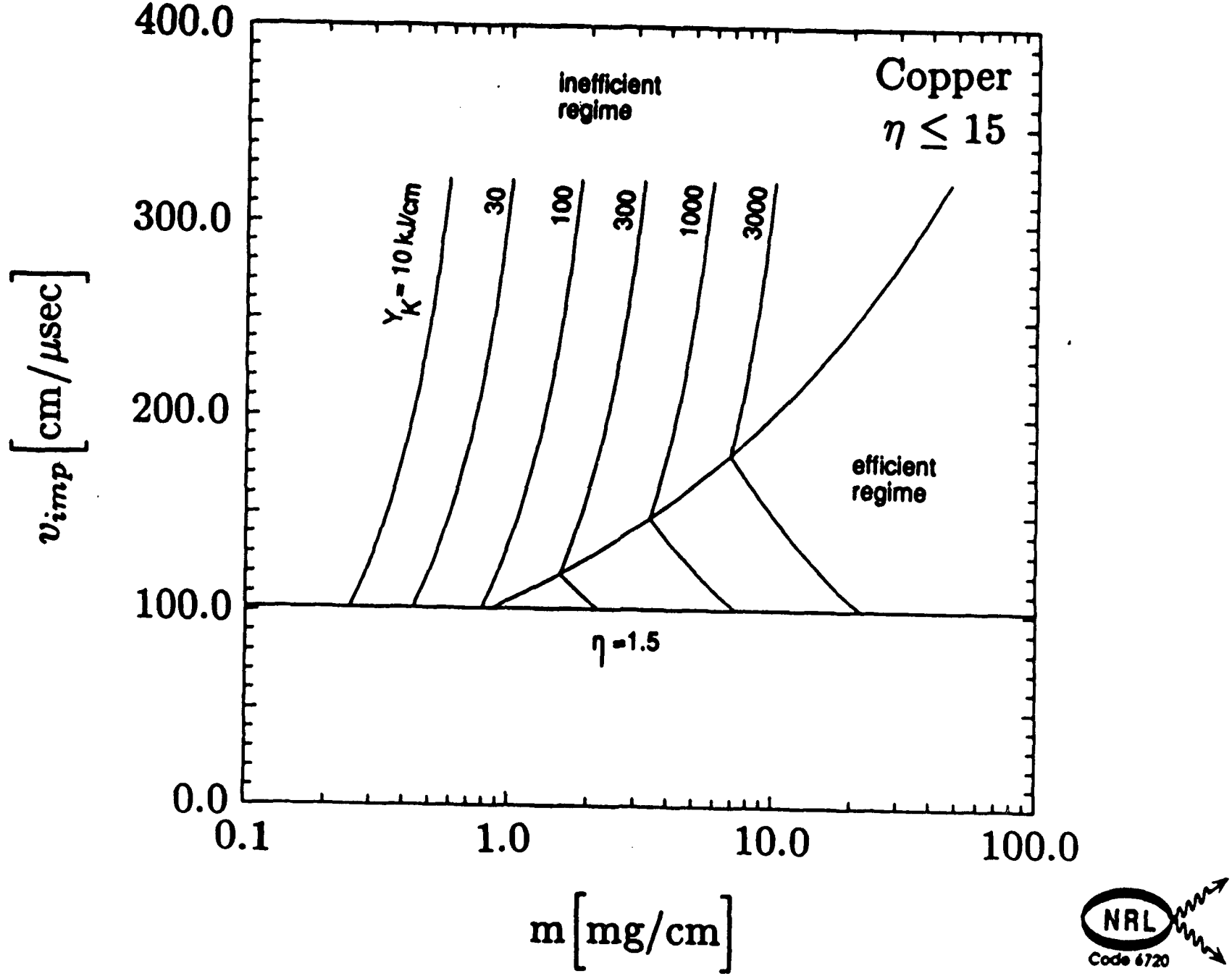
400.0
300.0
200.0
100.0
0.0
0.1
1.0
10.0
100.0
inefficient
regime
Copper
$\eta \leq 15$
Y_K= 10 kJ/cm
30
100
300
1000
3000
efficient
regime
η =1.5
v_{imp} [cm/μsec]
m [mg/cm]
NRL
Code 6720

Fig. 7

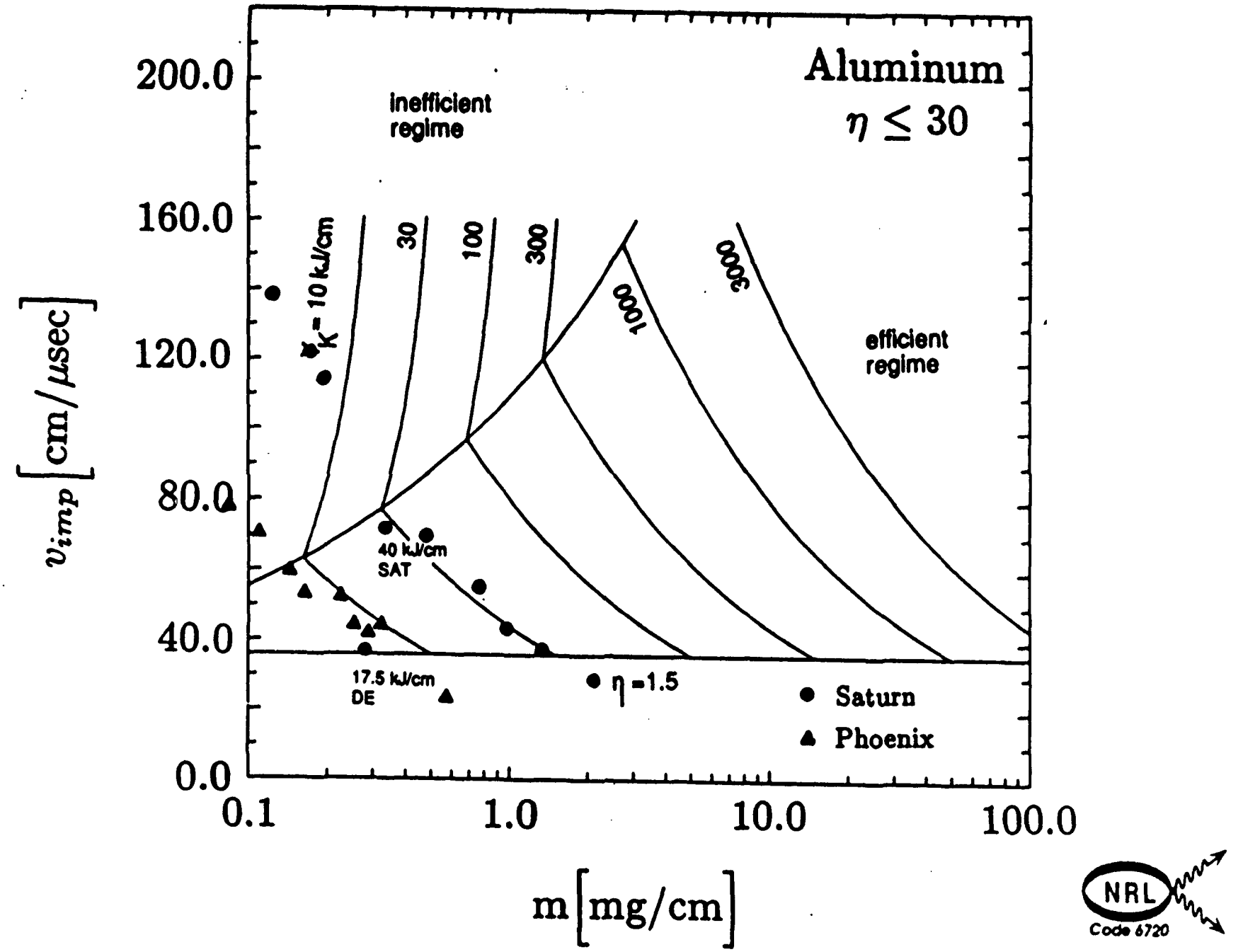
Aluminum
$\eta \leq 30$
inefficient regime
efficient regime
$K = 10$ kJ/cm
30
100
300
1000
3000
40 kJ/cm SAT
17.5 kJ/cm DE
$\eta = 1.5$
Saturn
Phoenix
200.0
160.0
120.0
80.0
40.0
0.0
0.1
1.0
10.0
100.0
$v_{imp}\left[\text{cm}/\mu\text{sec}\right]$
$m\left[\text{mg/cm}\right]$
NRL
Code 6720

Fig. 8

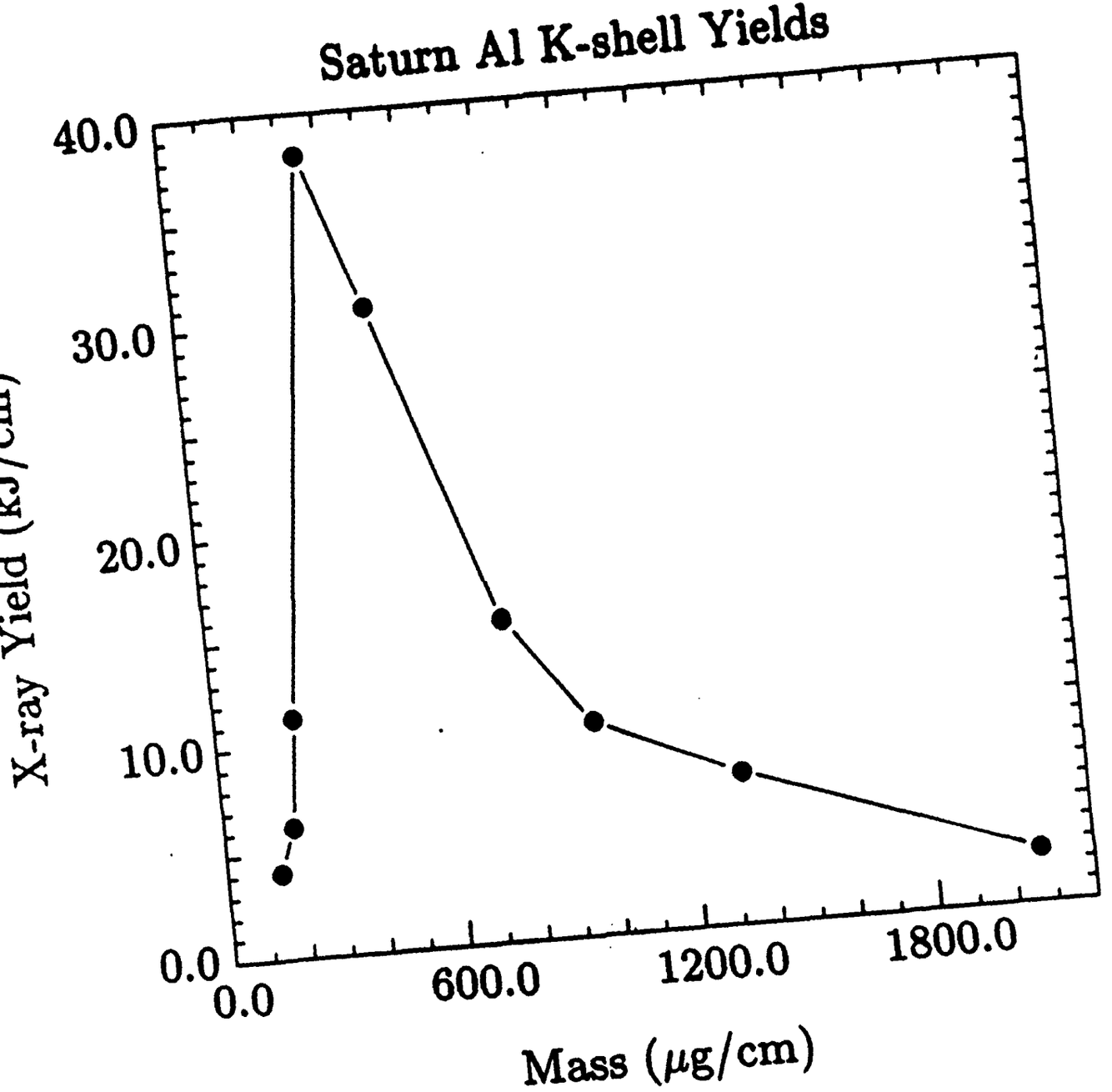
Saturn Al K-shell Yields
X-ray Yield (kJ/cm)
40.0
30.0
20.0
10.0
0.0
0.0
600.0
1200.0
1800.0
Mass (μg/cm)

Fig. 9

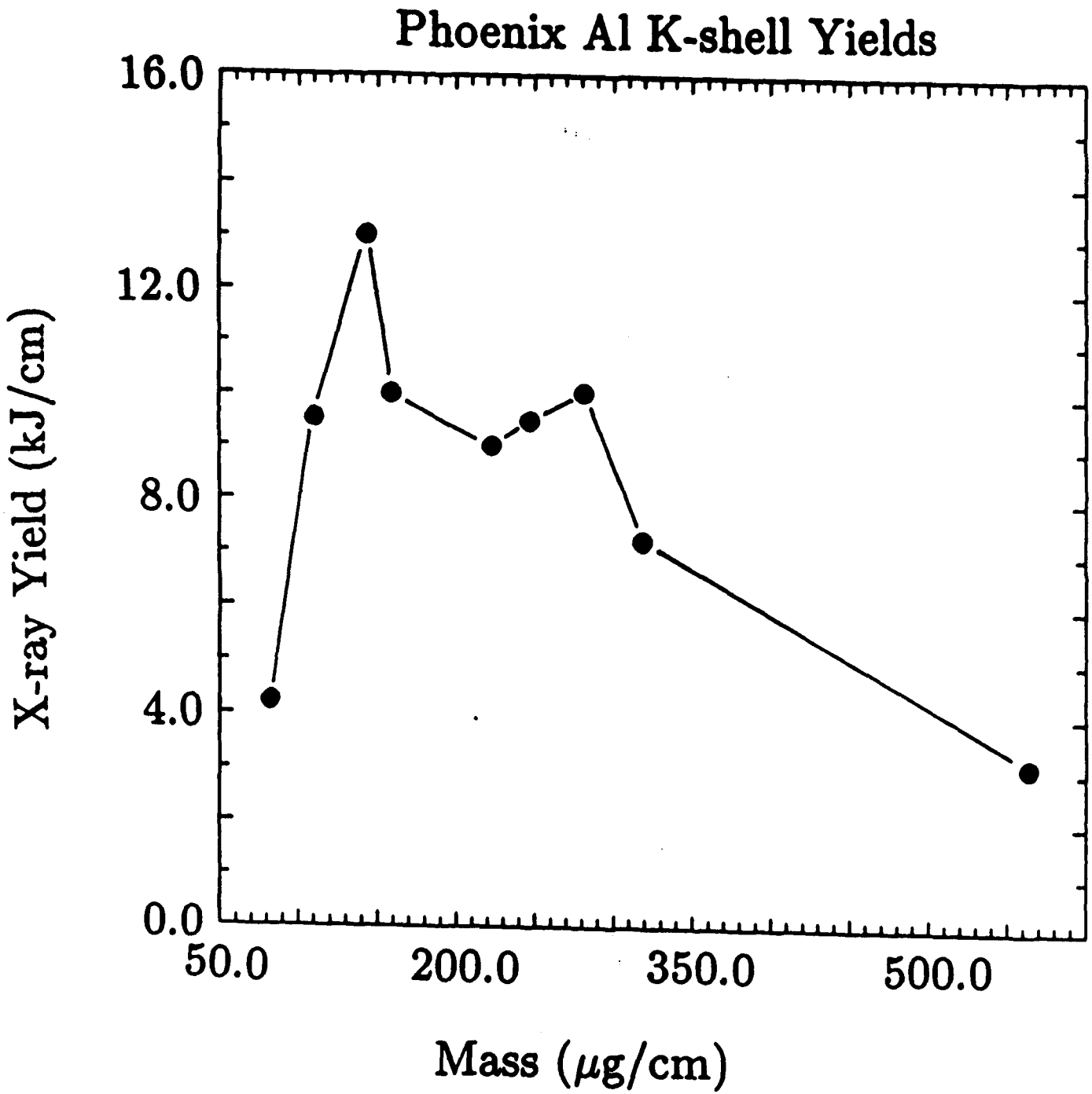
Phoenix Al K-shell Yields
16.0
12.0
8.0
4.0
0.0
X-ray Yield (kJ/cm)
50.0
200.0
350.0
500.0
Mass (μg/cm)

Fig. 10

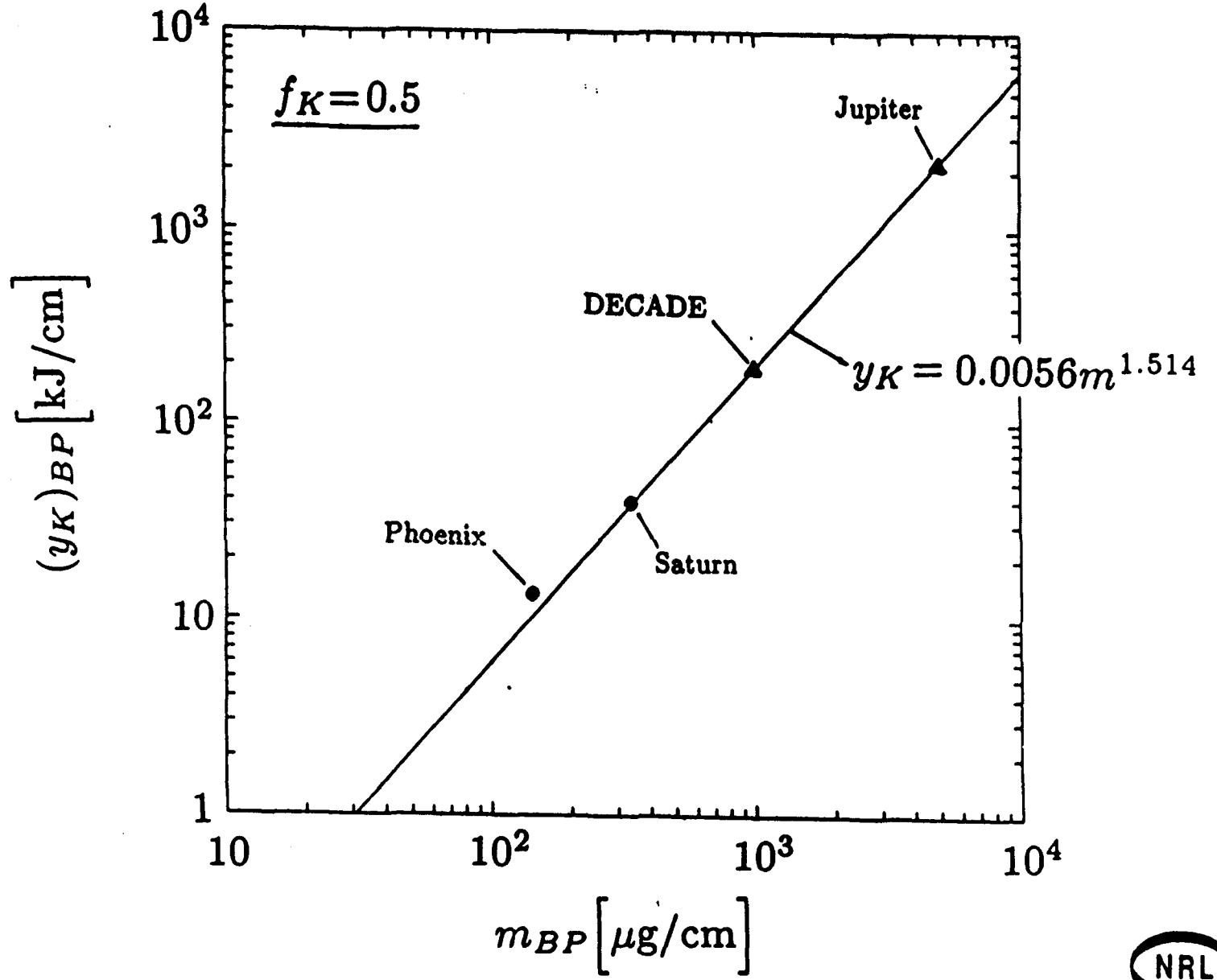

NRL
Code 6720

Fig. 11

Al K-Shell Yields for Different Machines Peak at a Similar Initial Wire Diameter

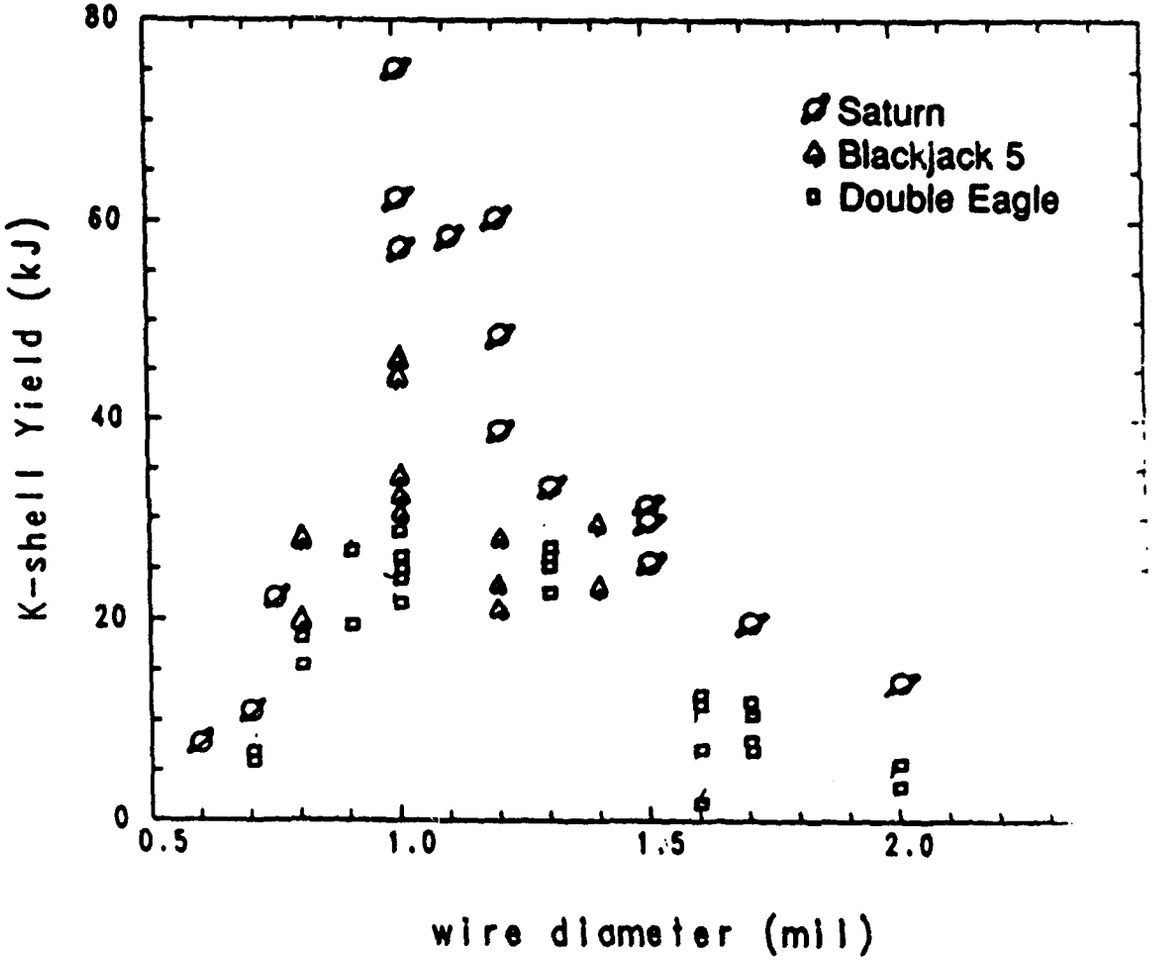

NRL
Code 6720

Fig. 12

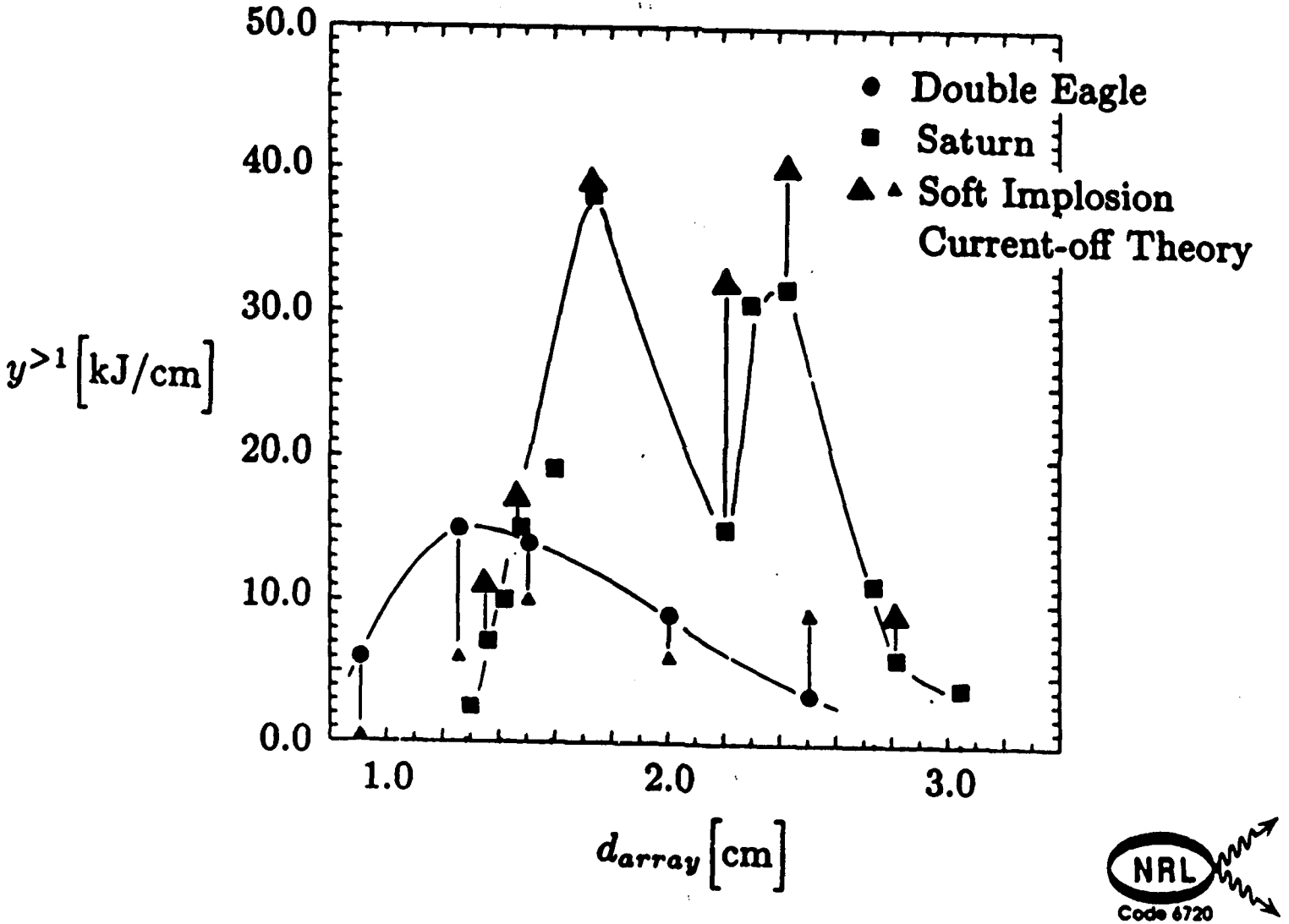
50.0
40.0
30.0
20.0
10.0
0.0
1.0
2.0
3.0
$y^{>1}$ [kJ/cm]
d_{array} [cm]
Double Eagle
Saturn
Soft Implosion
Current-off Theory
NRL
Code 6720

Fig. 13

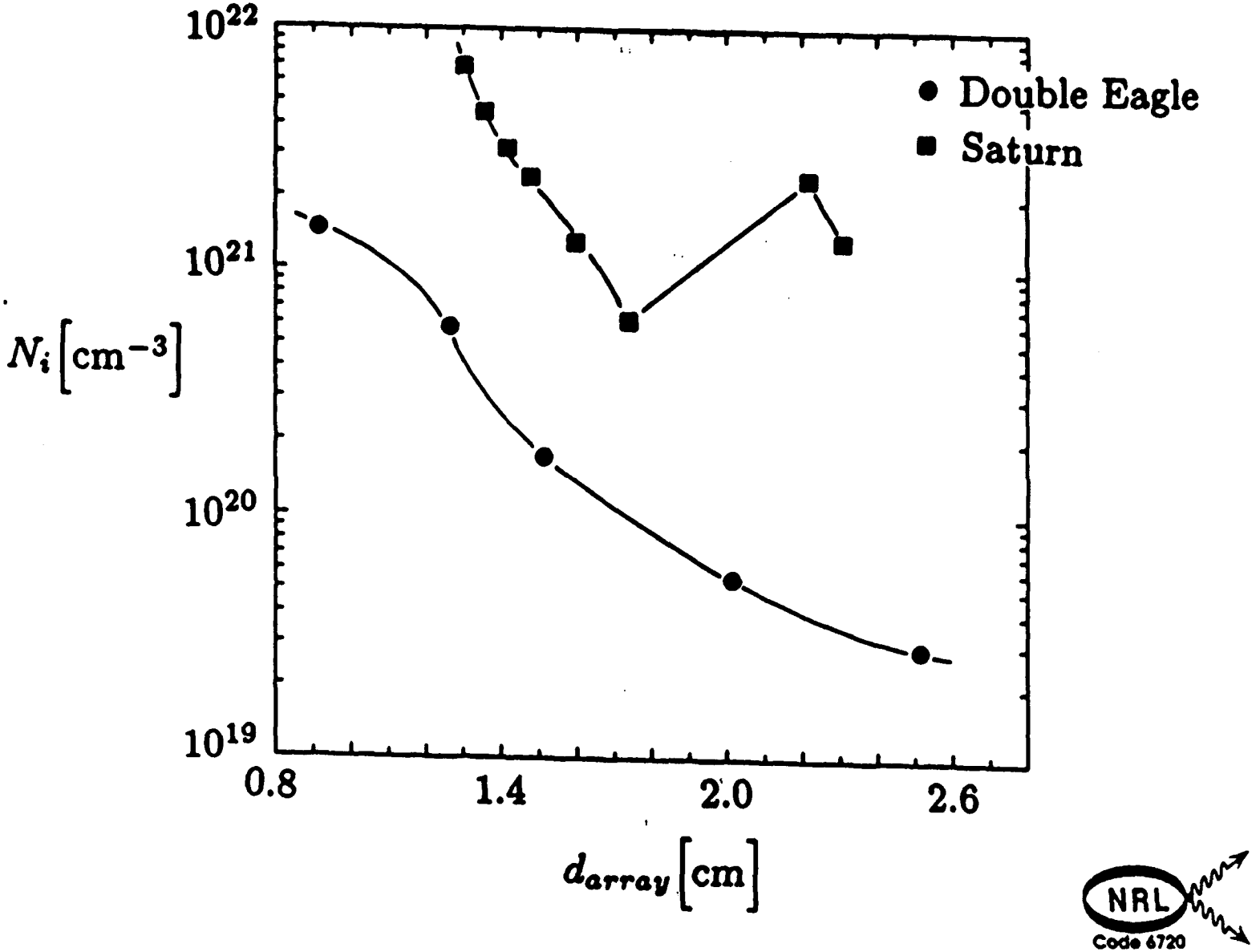
10^{22}
10^{21}
10^{20}
10^{19}
$N_i\left[\mathrm{cm}^{-3}\right]$
0.8
1.4
2.0
2.6
$d_{array}\left[\mathrm{cm}\right]$
Double Eagle
Saturn
NRL
Code 6720

Fig. 14

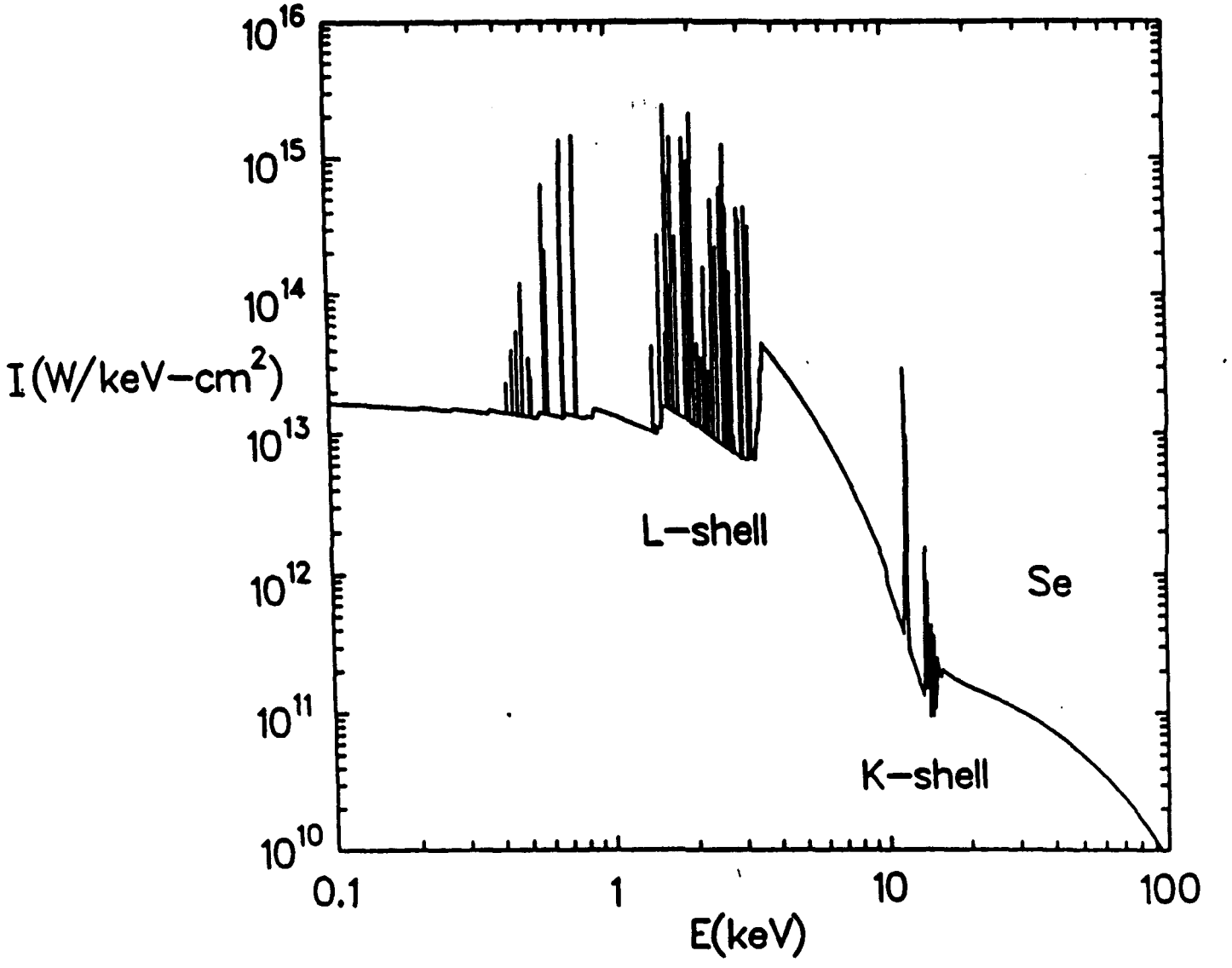
10^{16}
10^{15}
10^{14}
10^{13}
10^{12}
10^{11}
10^{10}
I(W/keV-cm^2)
L-shell
Se
K-shell
0.1
1
10
100
E(keV)
NRL
Code 6720

Fig. 15

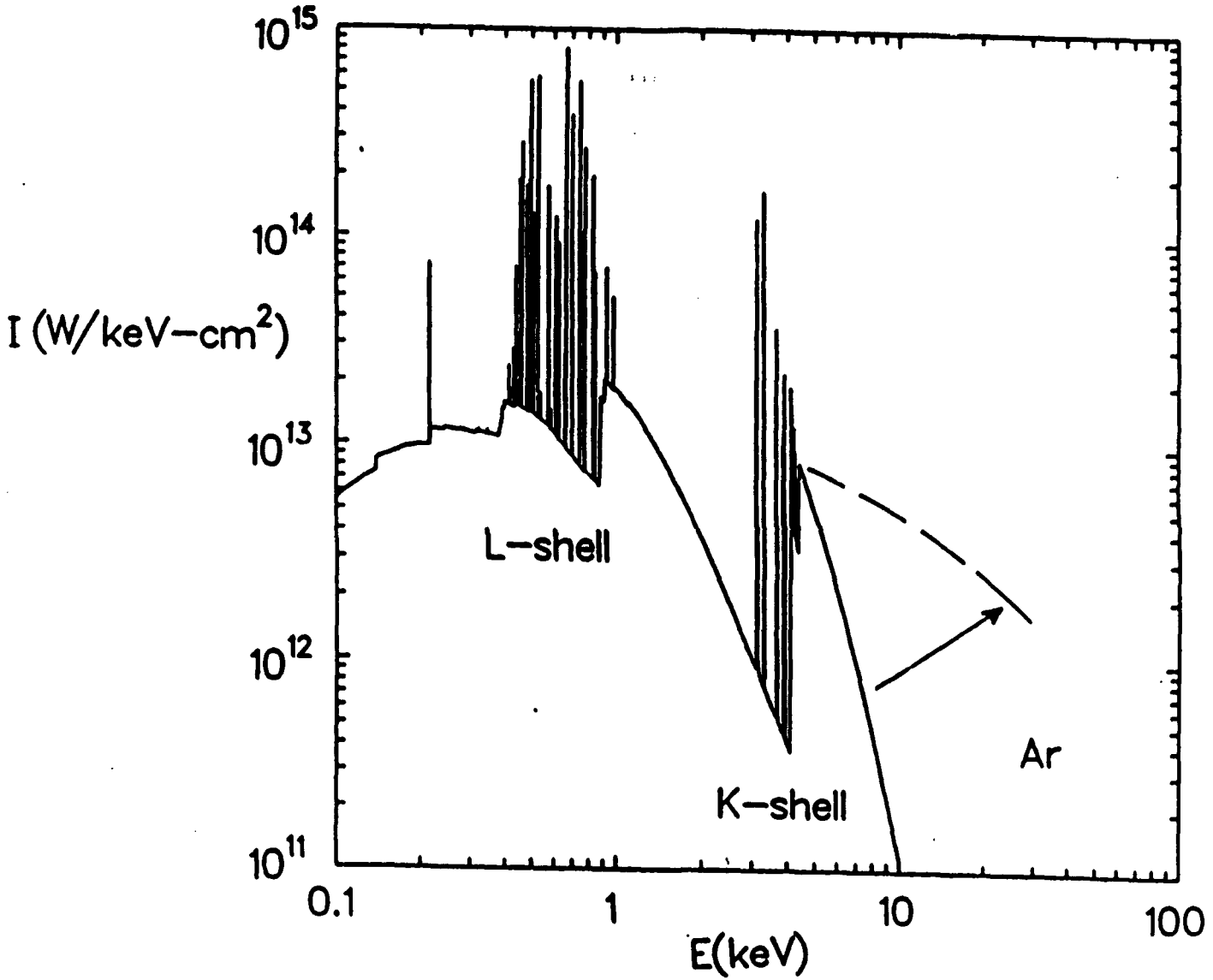

NRL
Code 6720

Fig. 16

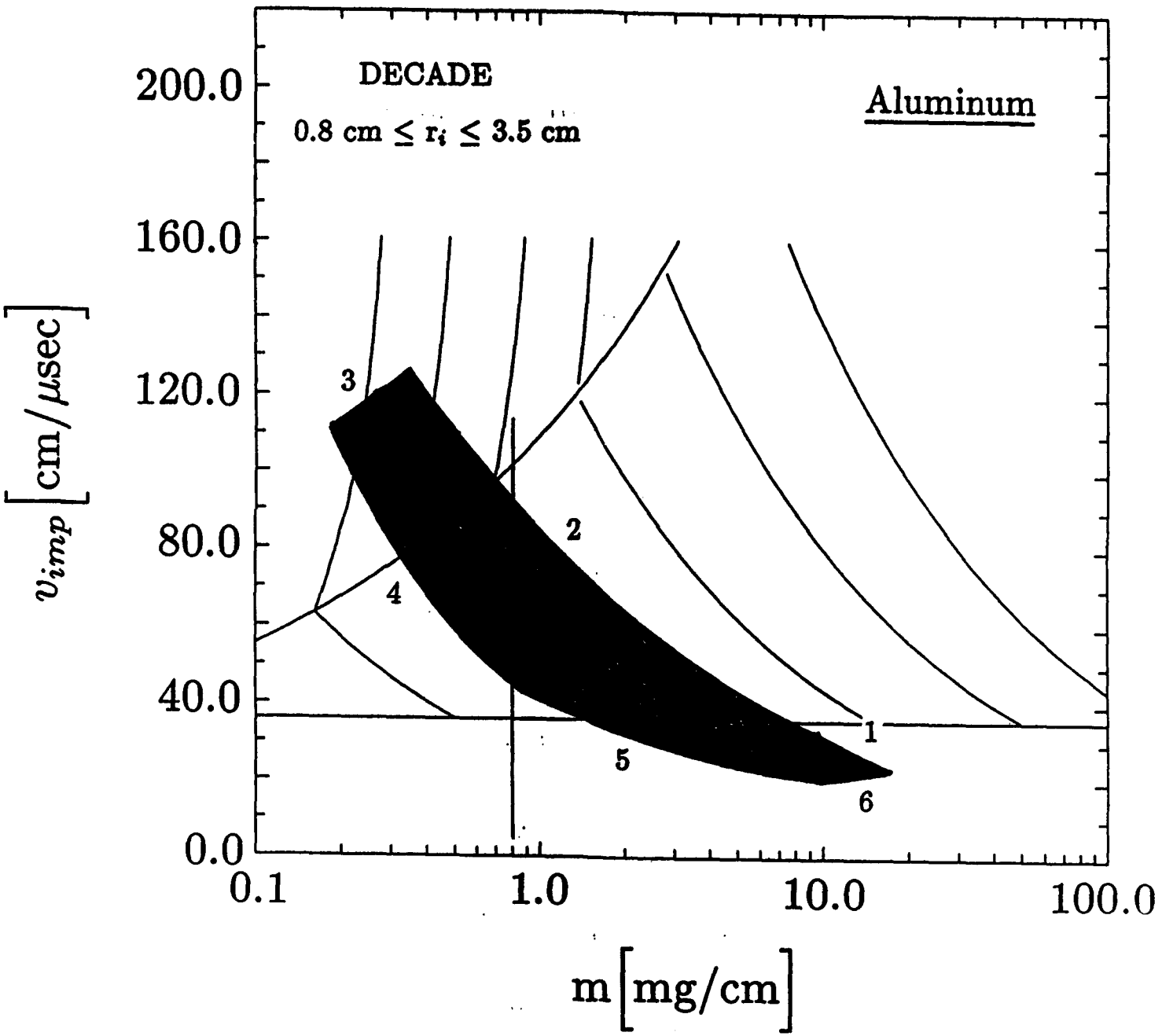
DECADE
0.8 cm ≤ r_i ≤ 3.5 cm
Aluminum
200.0
160.0
120.0
80.0
40.0
0.0
0.1
1.0
10.0
100.0
v_imp [cm/μsec]
m [mg/cm]
1
2
3
4
5
6

Fig. 17

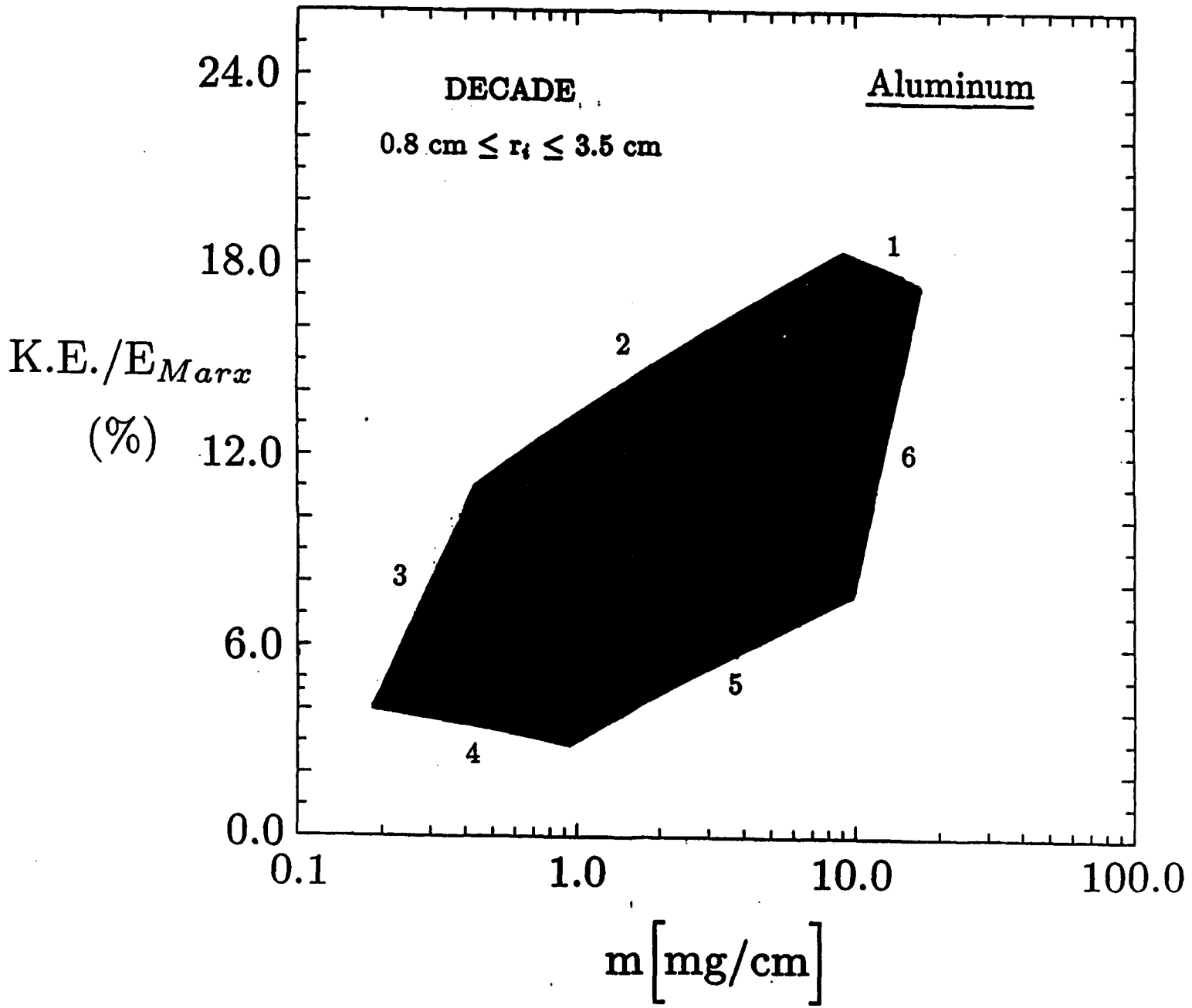
DECADE
Aluminum
0.8 cm ≤ r_f ≤ 3.5 cm
24.0
18.0
12.0
6.0
0.0
K.E./E_Marx
(%)
0.1
1.0
10.0
100.0
m[mg/cm]
1
2
3
4
5
6

Fig. 18